Thermochimica Acta 487 (2009) 60–64

Contents lists available at ScienceDirect

Thermochimica Acta

journal homepage: www.elsevier.com/locate/tca

Thermal and thermo-oxidative decomposition of ammonium–iron(II) phosphate monohydrate

Beatriz Ramajo[a], Aranzazu Espina[a], Nieves Barros[b], José R. García[c,*]

[a] Servicio de Termocalorimetría y Análisis Elemental, Servicios Científico-Técnicos, Universidad de Oviedo, 33006 Oviedo, Spain
[b] Departamento de Física Aplicada, Universidad de Santiago de Compostela, 15782 Santiago de Compostela, Spain
[c] Departamento de Química Orgánica e Inorgánica, Universidad de Oviedo, 33006 Oviedo, Spain

ARTICLE INFO

Article history:
Received 27 October 2008
Received in revised form 12 January 2009
Accepted 14 January 2009
Available online 22 January 2009

Keywords:
Thermal analysis
Model-free kinetics
Iron phosphates

ABSTRACT

The thermal and thermo-oxidative decompositions of $NH_4FePO_4{\cdot}H_2O$ were studied by means of a combination of classical thermal analysis techniques (TG and DSC) with MS and powder XRD analysis. The experiment was run in two different (inert and oxidizing) atmospheres. In an inert (N_2) atmosphere, thermal decomposition occurs in three steps at 265, 350 and 420 °C related to the evacuation of H_2O (steps 1 and 3) and NH_3 (steps 1–3). In an oxidizing (O_2) atmosphere, thermal evacuation is coupled with the oxidation from Fe(II) to Fe(III). In addition, application of Vyazovkin's model-free kinetic method to three TG curves obtained at different heating rates (5, 10 and 20 °C/min) allows the activation energy to be calculated as a function of the extent of conversion. This helps to disclose the kinetic scheme that facilitates understanding of the mechanism of these reactions.

1. Introduction

Ammonium phosphates of the general formula $NH_4M^{II}PO_4{\cdot}H_2O$ were first obtained by Debray [1]. These compounds have been used as pigments for protective paint finishes on metal and as fire retardants in paints and plastics [2,3]. They can be also used as fertilizers [4]. Moreover, as they are all only slightly soluble in water, they constitute slow-release fertilizers. In this respect, $NH_4FePO_4{\cdot}H_2O$ (AIP) has been proven effective in correcting iron deficiency (iron chlorosis) in plants grown in calcareous soils [5]. Plants need iron to survive and there is usually a lot of iron in the soil. However, this iron is in form of Fe(III) and is not available to plants [6,7]. So the effectiveness of iron phosphates as Fe fertilizers depends on their Fe(II) content, as has been demonstrated [8].

In recent years, kinetic investigations have constituted one of the most important applications of thermal analysis [9–11]. Usually, the solid-state reactions are not simple one-step processes and thus a combination of serial and parallel elementary steps should result in an activation energy that changes during the course of the reaction. The isoconversional (model-free) methods determine the activation energy from the common analysis of the multiple curves measured at different heating rates or at different isothermal temperatures. Moreover, model-free methods calculate the activation energy as a function of the extent of conversion. They thus help to disclose the complexity of a process and to identify its kinetic scheme [12–18].

The aim of this study is to further our knowledge in the mechanism of the $NH_4FePO_4{\cdot}H_2O$ thermo-oxidative degradation by using thermal analysis techniques, namely TG and DSC. Furthermore, the on-line study of evacuated gases in the TG experiment was carried out by mass spectrometric analysis. In addition, the activation energy as a function of the conversion is obtained by Vyazovkin's method by using TG data obtained at different heating rates.

2. Experimental

2.1. Synthesis and characterization

$NH_4FePO_4{\cdot}H_2O$ was obtained and characterized as described in a previous paper [5].

2.2. Thermal analysis procedures

A Mettler-Toledo TGA/SDTA851[e] and a DSC822[e] were used for the thermal analyses in nitrogen (or oxygen) dynamic atmosphere (50 mL/min) at a heating rate of 10 °C/min. For the kinetics measurements, the TG experiments were carried at heating rates of 5, 10 and 20 °C/min. In all cases, 10–12 mg of powder AIP sample was thermally treated. In TG tests, a Pfeiffer Vacuum ThermoStar™ GSD301T mass spectrometer was used to determine the evacuated vapours. The masses 18 (H_2O) and 15 (NH_3) were tested by using a detector C-SEM, operating at 1200 V, with a time constant of 1 s. The

* Corresponding author. Tel.: +34 985 103 030; fax: +34 985 103 446.
E-mail address: jrgm@uniovi.es (J.R. García).

0040-6031/$ – see front matter © 2009 Elsevier B.V. All rights reserved.
doi:10.1016/j.tca.2009.01.013

powder XRD of the residual solid char (sample heated up to 1000 °C) was performed on a Oxford Diffraction Geminis S diffractometer between 25° and 45° (2θ) in steps of 0.01° at a rate of 3 s step^{-1}, by using CuK_α radiation.

2.3. Kinetic parameters and modelling

The rate of heterogeneous solid-state reactions can generally be described by:

$$\frac{d\alpha}{dt} = k(T)f(\alpha) \quad (1)$$

where t is time, $k(T)$ the temperature-dependent constant and $f(\alpha)$ a function called the reaction model, which describes the dependence of the reaction rate on the extent of reaction, α.

The temperature dependence of the rate constant is described by the Arrhenius equation. Thus, the rate of a solid-state reaction can generally be described by:

$$\frac{d\alpha}{dt} = A\ e^{-E/RT} f(\alpha) \quad (2)$$

where A is the pre-exponential factor, E the activation energy and R the gas constant.

The preceding rate expression can be transformed into non-isothermal rate expressions describing reaction rates as a function of temperature at a constant heating rate, β:

$$\frac{d\alpha}{dT} = \frac{A}{\beta} e^{-E/RT} f(\alpha) \quad (3)$$

The use of several heating rates permits the application of model-free (isoconversional) methods. These methods make the assumption that the parameters of the model are identical for measurements at all heating rates. It allows a direct fit of the model to the experimental data without a transformation which would distort the error and hence the result [19]. An additional advantage lies in the fact that there are no limitations with respect to the complexity of the model; consequently, it is reliable in solving applied kinetic problems [19–21].

Vyazovkin and Sbirrazzuoli developed an isoconversional method [22]. Integrating up to conversion, α, Eq. (3), gives:

$$\int_0^\alpha \frac{d\alpha}{f(\alpha)} = g(\alpha) = \frac{A}{\beta} \int_{T_0}^{T} e^{-E/RT} dT \quad (4)$$

As $E/2RT \gg 1$, the temperature integral can be approximated by:

$$\int_{T_0}^{T} e^{-E/RT}\, dT \approx \frac{R}{E} T^2\, e^{-E/RT} \quad (5)$$

Substituting the temperature integral and taking the logarithm gives:

$$\ln \frac{\beta}{T_\alpha^2} = \ln \left[\frac{RA}{E_\alpha g(\alpha)} \right] - \frac{E_\alpha}{R} \frac{1}{T_\alpha} \quad (6)$$

To apply the method, it is necessary to obtain at least three different heating rates (β), the respective conversion curves being subsequently evaluated from the measured TG curves [22,23]. For each conversion (α), $\ln(\beta/T_\alpha^2)$ plotted against $1/T_\alpha$, gives a straight line with slope $-E_\alpha/R$. Thus, the activation energy is obtained as a function of the conversion.

3. Results and discussion

The TG/DTG curves of AIP obtained in an inert (N_2) atmosphere are shown in Fig. 1a. TG curve consist of two continuous stage mass loss processes. The total mass loss up to 1000 °C is 22.0% (cal. 23.5%). The DTG curve shows two minima (265 and 420 °C) at higher temperatures that the previously described for $NH_4FePO_4{\cdot}H_2O$ nano-plates thermal decomposition (105 and 218 °C, respectively) [24], probably as a consequence of the very different particle size of both samples. The powder XRD of the residual solid char correspond to β-$Fe_2P_2O_7$ [25].

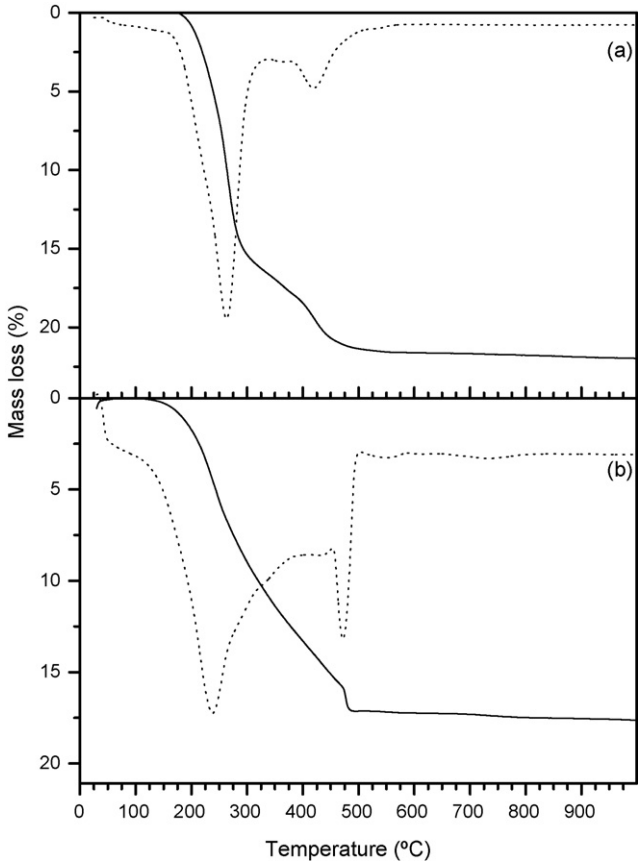

Fig. 1. TG (—) and DTG (···) curves of $NH_4FePO_4{\cdot}H_2O$ obtained in a N_2 (a) or O_2 (b) atmosphere.

The associated mass spectrometric analysis is reported in Fig. 2a. The mass spectrometric m/z 18 curve (associated with water evacuation) has two maxima, while the mass spectrometric m/z 15 curve has three (associated with ammonia evacuation). This fact reveals a small band in the DTG curve with a minimum at 350 °C associated with the second step of elimination of ammonia molecules. Integration of the bands into the ion current curve permits the mass loss associated with each step to be calculated. Results indicate that the process commences with the loss of 12% of water and 6% of ammonia (265 °C). It then proceeds (350 °C) with the loss of 1% ammonia. Finally, thermal evacuation is completed with the loss of the rest of the water (3%) and ammonia (5%). As the mass spectrometer was not calibrated for quantitative analysis, these calculations are semi-quantitative. Nonetheless, the TG/DTG and masses analyses are in good agreement.

Fig. 3a shows the conversion curves of the thermal decompositions of AIP at three different heating as a function of the temperature. It can be observed that the heating rate does not affect the mass loss, although it does have an effect on the shape of the two TG and conversion curves, which moves to higher temperatures as the heating rate increases. Application of Vyazovkin's model-free method to these curves leads to the calculation of the variation in activation energy (E) as a function of the conversion degree (see Fig. 4). E is approximately constant in the conversion range of 10–35% (E = 80 kJ/mol), and increases until ~130 kJ/mol (conversion = 55–60%). Later on, it diminishes until ~100 kJ/mol

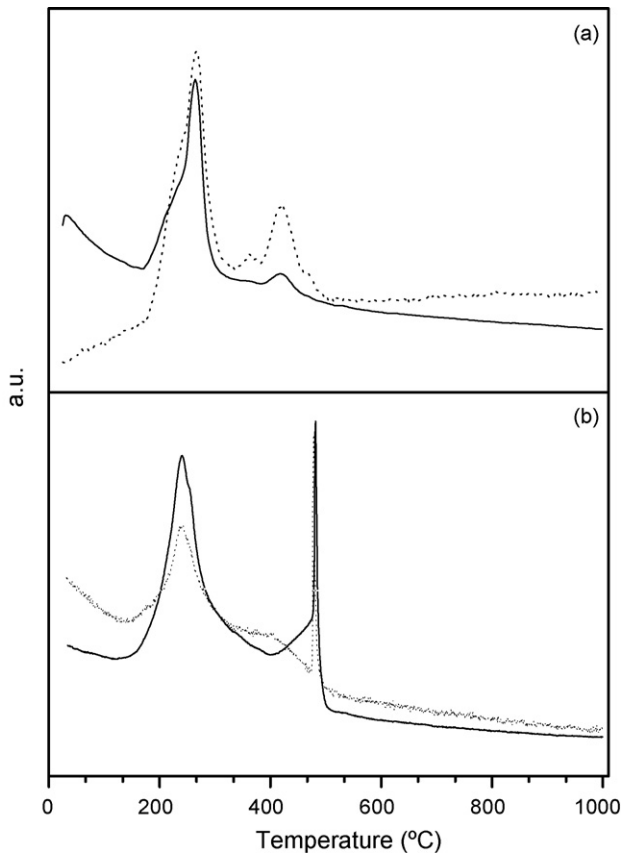

Fig. 2. m/z 18 (H_2O (—)) and m/z 15 (NH_3 (···)) MS signals of evacuated vapours by $NH_4FePO_4{\cdot}H_2O$ in a N_2 (a) or O_2 (b) atmosphere.

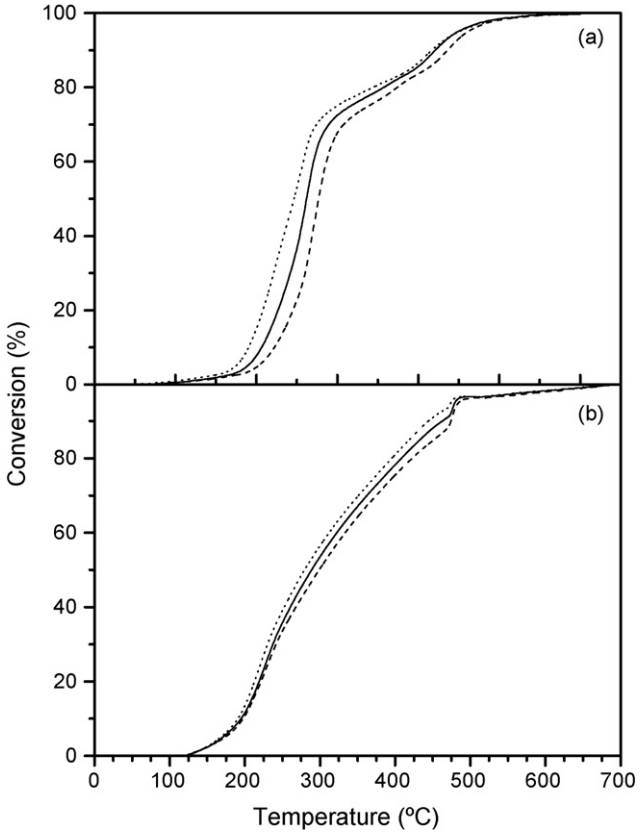

Fig. 3. Conversion curves of $NH_4FePO_4{\cdot}H_2O$ in a N_2 (a) or O_2 (b) atmosphere as a function of heating rate: 5°C/min (···), 10°C/min (—) and 20°C/min (---).

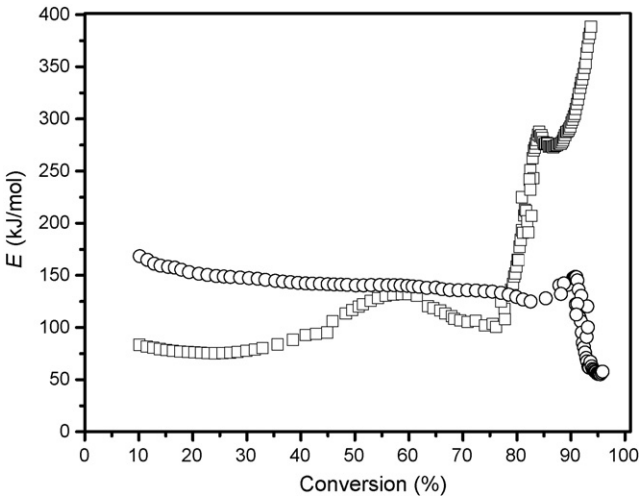

Fig. 4. Dependence of the activation energy on the extent of conversion in the $NH_4FePO_4{\cdot}H_2O$ thermal decomposition: N_2 (○) or O_2 (□) atmosphere.

(conversion = 70–75%) before increasing again. In general, constant E-values can be expected in the case of a single reaction. However, in our experiment, the E_α curve sinusoidal profile indicates that the decomposition mechanism is a function of the conversion degree. This fact should be related to the difference in both water and ammonia desorption steps. Finally, from 75% of conversion on, the E-values continually increase probably due to the liberation of water and ammonia trapped inside the β-$Fe_2P_2O_7$ 3D-structure.

The TG/DTG curves of AlP obtained in a reactive (O_2) atmosphere are presented in Fig. 1b and show that the mass loss up to 1000 °C is 17.6% (cal. 19.3%). The product of reaction is α-$FePO_4$ [26].

The associated mass spectrometric analysis is reported in Fig. 2b. As in an inert atmosphere (see Fig. 2a), the mass spectrometric m/z 18 (H_2O) curve has two maximums, but the two MS-curve profiles are very different. Hence, the mechanism of thermal evacuation is different in both atmospheres: N_2 and O_2. Fig. 4 shows the variation in activation energy with the conversion of the decomposition/oxidation reaction obtained through the application of Vyazovkin's model-free method to three TG curves at different heating rates (Fig. 3b). Until 90% conversion, E has a value of ∼150 kJ/mol, while from 90% of conversion to the end the E-value diminishes abruptly. This drop in E-values leads to acceleration of the process,

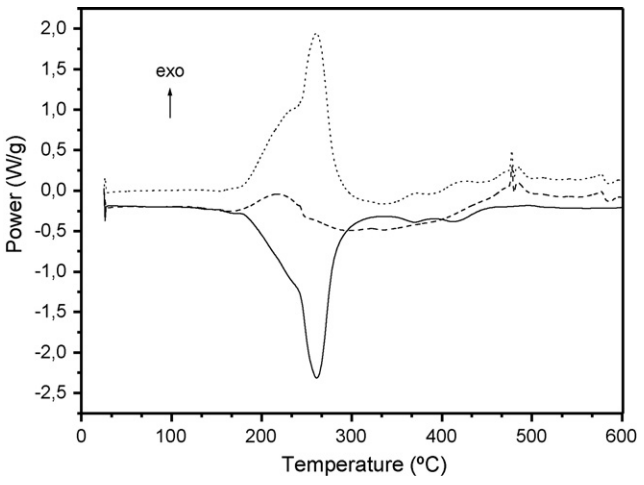

Fig. 5. DSC curves of $NH_4FePO_4{\cdot}H_2O$ obtained in a N_2 (—) or O_2 (---) atmosphere and their difference (···).

which can be seen in the TG curve as an instantaneous 2% mass loss at 457 °C (heating rate 10 °C/min).

Fig. 5 shows the DSC curves obtained for AIP. Up until 160 °C, both curves run together. Subsequently, in a N_2 (inert) atmosphere, there are three endothermic peaks at 260, 370 and 410 °C associated with the three steps of evacuation of ammonia and water molecules. In an O_2 (oxidizing) atmosphere, the endothermic desorption process is coupled with the Fe(II) → Fe(III) oxidation, which is an exothermic phenomenon. Consequently, the shape of the DSC curve is very different and shows a number of diverse exothermic signals in the temperature range between 160 and 460 °C. Furthermore, the DSC curve in an O_2 atmosphere presents a very complex exothermic signal between 460 and 500 °C. This is related to the loss of the last fraction of water and ammonia, to the Fe(II) → Fe(III) oxidation and also to the crystallisation of the polymorph α-$FePO_4$ [27]. Finally, there is a small exothermic signal around 560 °C that is probably related to the thermo-oxidative decomposition of a small fraction of remaining AIP. This can be seen in the DTG curve (see Fig. 1b) as a very small band at 560 °C which is not considered in the previously proposed mechanism.

The preceding results lead to the following observations: (i) In our synthesis conditions, AIP is stable until 160 °C. Above this temperature, evacuation of water and ammonia begins. This fact is independent of the atmosphere type. (ii) In an O_2 atmosphere, oxidation from Fe(II) to Fe(III) commences at 160 °C, as water and ammonia evacuation. (iii) The evacuation process is different in

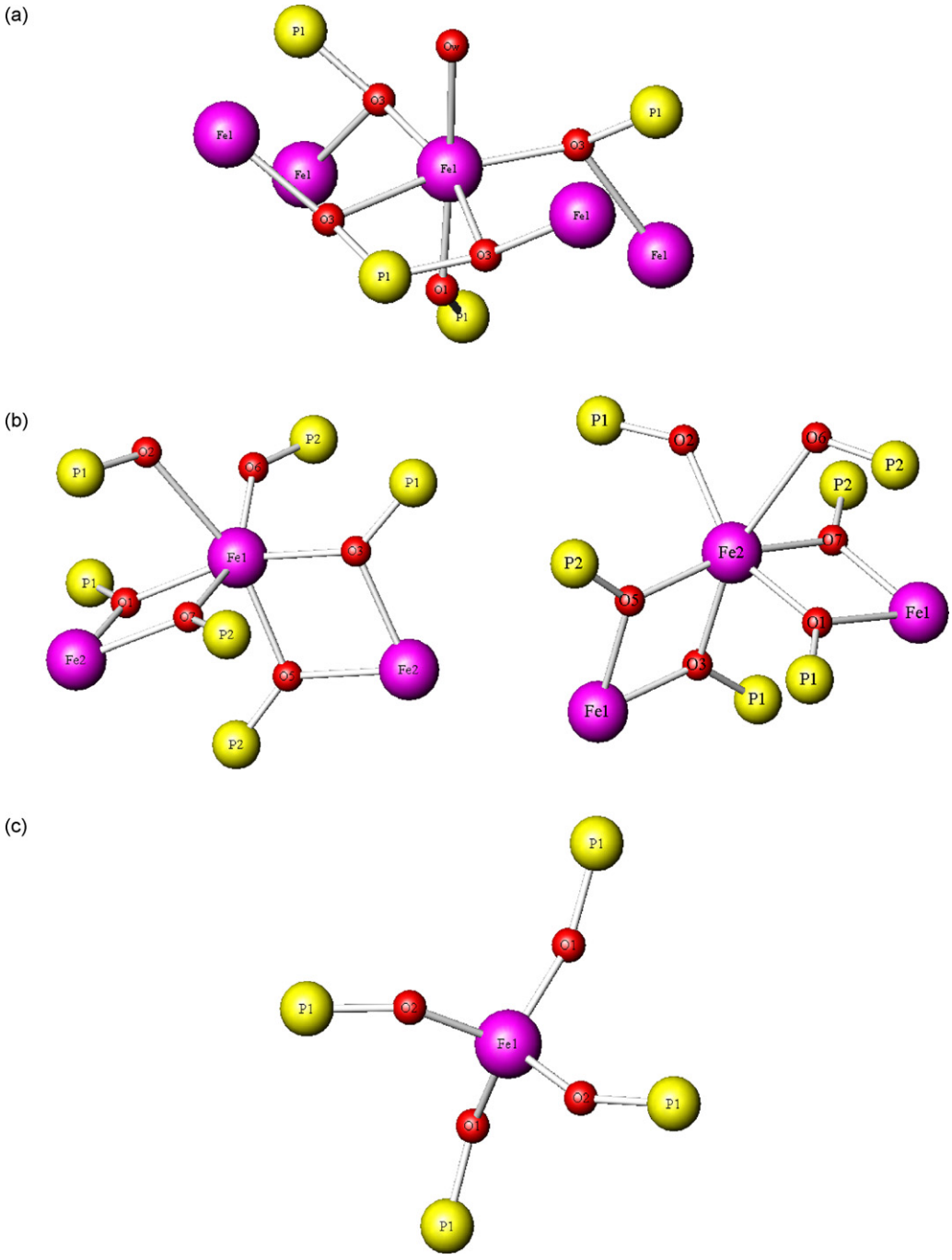

Fig. 6. Coordination environment about Fe atom in $NH_4FePO_4{\cdot}H_2O$ (a), β-FeP_2O_7 (b), and α-$FePO_4$ (c). Fe: magenta, P: yellow, O: red. (For interpretation of the references to color in this figure legend, the reader is referred to the web version of the article.)

both atmospheres, N_2 or O_2, with formation of β-$Fe_2P_2O_7$ or α-$FePO_4$, respectively.

Layered $NH_4FePO_4{\cdot}H_2O$ crystallizes in the orthorhombic space group *Pmm*21 [28]. The structure consists of approximately square–planar sheets of iron(II) ions, coordinated in a severely distorted octahedron by five phosphate oxygen molecules and one water molecule (see Fig. 6a). The negatively charged layers are bound by hydrogen bonds, with participation of interlayer ammonium cations. When AIP is heated up to 160 °C, thermal decomposition begins regardless of the atmosphere employed. In an inert (N_2) atmosphere, the evacuation of water and ammonia molecules leads to the formation of β-$Fe_2P_2O_7$, where the Fe-octahedral coordination is preserved (see Fig. 6b). In the presence of O_2, the iron(II) oxidation occurs in parallel with the evacuation process. A qualitative visualization can be made through the DSC curve obtained by the difference between both (N_2 and O_2) DSC curves, presented in Fig. 5. This curve shows that most of the oxidation occurs between 200 and 320 °C. Integration of the curve in this temperature range allows an exothermic signal of 120 kJ/mol to be calculated. Probably, a pseudolayered habit is maintained until 475 °C and, at this temperature, α-$FePO_4$ is crystallized and the quick structural reorganization is detected by DSC (in opposition, the β-$Fe_2P_2O_7$ formation takes place simultaneously to the AIP decomposition, what explains the absence of an isolated exothermic signal in the N_2-DSC curve). In the thermo-oxidative decomposition of AIP, the environment of iron is drastically modified, going from six- to four-coordination (see Fig. 6c). This "structurequake" should be responsible of the high *E*-values for the AIP thermal decomposition in O_2 atmosphere.

4. Conclusions

The thermal and thermo-oxidative decompositions of $NH_4FePO_4{\cdot}H_2O$ were studied by means of a combination of classical thermal analysis techniques (TG and DSC) with MS and powder XRD analysis. In an inert atmosphere, thermal decomposition appears to have a three-step mechanism with the evacuation of water and ammonia and the formation of β-$Fe_2P_2O_7$. In an oxidizing atmosphere, oxidation of iron(II) takes places in parallel to the evacuation process. Thermo-oxidative decomposition ceases with the crystallization of α-$FePO_4$.

Application of Vyazovkin's model-free kinetic method allows the activation energy to be calculated as a function of the extent of conversion. This helps to identify the kinetic scheme that facilitate understanding of the mechanism of these reactions.

Acknowledgments

This work has been carried out with the financial support of FEDER-MEC (MAT2006-01997, and Factoría Española de Cristalización–Consolider Ingenio 2010) and the Gobierno del Principado de Asturias (PC-06-020).

References

[1] H. Debray, Ann. Chim. Phys. 61 (1961) 437.
[2] A.M. Erskine, G. Grim, S.C. Horning, Ind. Eng. Chem. 36 (1944) 456.
[3] S.I. Vol'fkovich, R.E. Remen, Chem. Abstr. 50 (1956) 6243.
[4] G.L. Bridger, M.L. Salutsky, R.S. Starostka, J. Agric. Food Chem. 10 (1962) 181.
[5] N. Barros, C. Airoldi, J.A. Simoni, B. Ramajo, A. Espina, J.R. García, Thermochim. Acta 441 (2006) 89.
[6] V. Römheld, H. Narschner, Plant Physiol. 71 (1983) 949.
[7] W. Schmidt, New Phytol. 141 (1999) 1.
[8] V. Barrón, J. Torrent, J. Agric. Food Chem. 42 (1994) 105.
[9] S. Vyazovkin, N. Sbirrazzuaoli, Macromol. Rapid Commun. 27 (2006) 1515.
[10] S. Vyazovkin, Anal. Chem. 80 (2008) 4301.
[11] Recent advances, techniques and applications Handbook of Thermal Analysis and Calorimetry, vol. 5, Elsevier, Amsterdam, 2008.
[12] S. Vyazovkin, Int. J. Chem. Kinet. 28 (1996) 95.
[13] S. Vyazovkin, C.A. Wight, Int. Rev. Phys. Chem. 17 (1998) 407.
[14] M.E. Brown, M. Maciejewski, S. Vyazovkin, R. Nomen, J. Sempere, A. Burnham, J. Opfermann, R. Strey, H.L. Anderson, A. Kemmler, R. Keuleers, J. Janssens, H.O. Desseyn, C.-R. Li, T.B. Tang, B. Roduit, J. Malek, T. Mitsuhashi, Thermochim. Acta 355 (2000) 125.
[15] M. Maciejewski, Thermochim. Acta 355 (2000) 145.
[16] S. Vyazovkin, Thermochim. Acta 355 (2000) 155.
[17] A.K. Burnham, Thermochim. Acta 355 (2000) 165.
[18] J.R. Opfermann, Thermochim. Acta 391 (2002) 119.
[19] K. Zhang, J. Hong, G. Cao, D. Zhan, Y. Tao, C. Cong, Thermochim. Acta 437 (2005) 145.
[20] G.J.T. Fernandes, A.S. Araújo, V.J. Fernandez Jr., Cs. Novak, J. Therm. Anal. Calorim. 75 (2004) 687.
[21] G.T. Mohanraj, T. Vikram, A.M. Shanmugharaj, D. Khastgir, T.K. Chaki, J. Mater. Sci. 41 (2006) 4777.
[22] S. Vyazovkin, N. Sbirrazzuoli, Anal. Chim. Acta 355 (1997) 175.
[23] S. Vyazovkin, C.A. Wight, Annu. Rev. Phys. Chem. 48 (1997) 125.
[24] A.Q. Yuan, J. Wu, Z.Y. Huang, S. Liao, Zh.F. Tong, Mater. Res. Bull. 43 (2008) 1339.
[25] C. Parada, J. Perles, R. Sáez-Puche, C. Ruiz-Valero, N. Snejko, Chem. Mater. 15 (2003) 3347.
[26] J. Haines, O. Cambon, S. Hull, Z. Kristallogr. 218 (2003) 193.
[27] Y. Song, S. Yang, P.Y. Zavalij, M.S. Whittingham, Mater. Res. Bull. 37 (2002) 1249.
[28] S.G. Carling, P. Day, D. Visser, Inorg. Chem. 34 (1995) 3917.